River Flow 2016 – Constantinescu, Garcia & Hanes (Eds)
© 2016 Taylor & Francis Group, London, ISBN 978-1-138-02913-2

A 3D flow calculation around a structure in gravel bed rivers by using non-hydrostatic depth-integrated model with dynamic rough-wall law

T. Uchida & S. Fukuoka
Research and Development Initiative, Chuo University, Tokyo, Japan

A.N. Papanicolaou
Department of Civil and Environmental Engineering, The University of Tennessee, Knoxville, TN, USA

ABSTRACT: A reliable depth-integrated model is required for practical application to rivers. This paper presents a non-hydrostatic depth-integrated model of the general Bottom Velocity Computation (BVC) method that employs dynamic wall law (BVC-DWL) to calculate 3D flow calculations around a structure in gravel bed rivers. We applied the BVC-DWL method to a local 3D flow around a structure measured in a field experiment using an enhanced measurement method with the Acoustic Doppler Current Profiler (ADCP). The BVC-DWL method is validated for local 3D flow around structures in gravel bed rivers though comparisons with measured data, demonstrating the advantages of introducing the DWL instead of the conventional equilibrium wall law. This paper presents the non-equilibrium flow structures near the gravel bed around a structure in the calculation results, and discusses the limitations of the conventional rough-wall law and the necessity of introducing a dynamic rough-wall law.

1 INTRODUCTION

Recent advances in computational technology and developments of numerical schemes allow us to calculate 3D flows around structures in rivers. The conventional equilibrium wall law that assumes an equilibrium flow condition near the bed and employs a function of shear velocity and lowest velocity is not suitable as a boundary condition for gravel bed rivers, since the non-equilibrium flow near the bed causes vertical momentum fluxes near the bed. Some researchers have developed new methods with a 3D flow calculation model that treats bed material as a permeable resistance, instead of assuming the impermeable surface bed for the conventional method, and calculates the non-equilibrium motion near the bed surface and in the roughness layer under the bed surface (Olsen and Stokseth, 1995; Lane et al., 2004; Carney et al., 2006; Nicora et al, 2007a, 2007b; Rameshwaran et al., 2011).

While we recognize the need for a non-hydrostatic three-dimensional method for this purpose, a reliable depth-integrated model is also required for practical applications to rivers. In fact, the applications of a 3D model to river flows have been limited to small-scale laboratory experiments owing to its large computational cost. However, for a depth-integrated model, which has been developed for applications to actual river flows, there remains the challenge of developing an evaluation method for non-equilibrium fluid motions near the gravel bed, as indicated above for a 3D calculation method. One reason for this is that most previous depth-integrated models, including quasi-three-dimensional models, have been simplified with the assumption of the hydrostatic pressure distribution (Ishikawa et al., 1986; Fukuoka et al., 1992; Jin & Steffler 1993; Yeh and Kennedy, 1993).

Recently we developed a new quasi-three-dimensional calculation method without a shallow-water assumption such as hydrostatic pressure distribution. This new approach is called the general Bottom Velocity Computation (BVC) method, in which equations for velocity and pressure distributions in the vertical direction are solved with depth averaged velocity equations (Uchida & Fukuoka, 2012, 2014). The BVC method has been validated for several flows including rapidly varied flows over a structure and three-dimensional flows around a non-submerged structure where the horseshoe vortex is prominent (Fukuoka & Uchida, 2013). However, it is still challenging to calculate the velocity distribution near the bed for the 3D flow around structures by using the depth-integrated model including the BVC method. The key to overcoming this issue is assumed on the bottom boundary conditions for depth-integrated equations of the BVC method. Uchida et al. (2014) proposed the dynamic wall law for rough bed (DWL) by introducing continuity and momentum equations for vortex and

roughness layers. The BVC method employing the dynamic wall law (BVC-DWL) demonstrated the ability to calculate velocity distribution over a rough bed with isolated boulders in an experimental channel. However, the BVC-DWL method has not been validated for flows in gravel bed rivers.

The objective of this paper is to discuss the validity of the BVC-DWL method for a 3D flow around a structure in a gravel bed river. We applied the BVC-DWL method to the local 3D flow around a structure measured in a field experiment with the enhanced measurement method using the Acoustic Doppler Current Profiler (ADCP) (Koshiishi et al., 2012; 2013). The calculation results of the BVC-DWL method were compared with the measured data, demonstrating the advantages of introducing the DWL instead of the conventional equilibrium wall law (BVC-EWL).

2 CALCULATION METHODS

2.1 *Framework of BVC-DWL method*

In this method, the computational domain is separated in the vertical direction into the main computational domain and the wall-law layer near the bed, as shown in Figure 1. For the main computational domain between the water surface and the top of the wall-law layer, we refined the BVC method, which is an advanced non-hydrostatic depth-integrated model composed of horizontal momentum equations and several equations for vertical velocity and pressure distributions (Figure 2), to take into account the momentum transfer at the top of the wall law layer owing to non-equilibrium flow near the bed. The wall law layer is composed of a vortex layer and a roughness layer. As a dynamic boundary condition of the rough bed, this method employs continuity and momentum equations for these layers (Table 1). The momentum equations have been derived so that this method reduces to the conventional equilibrium rough-wall law for the uniform flow condition, as indicated in the following section.

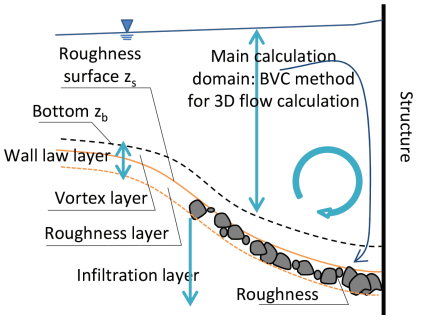

Figure 1. Framework of the present flow calculation method with dynamic rough wall law (BVC-DWL).

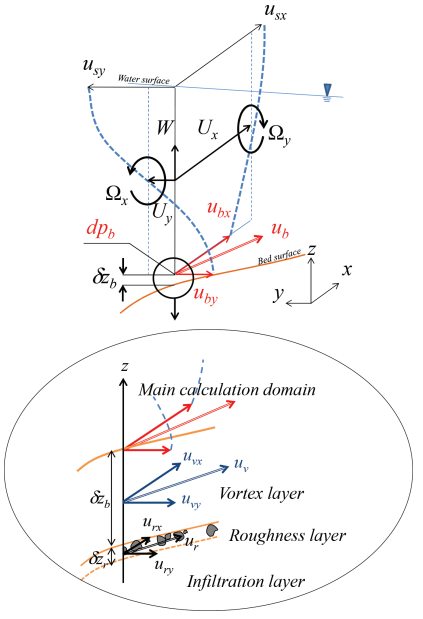

Figure 2. Unknown variables in the main calculation domain of BVC-DWL method.

2.2 *Equations for main computational domain (general bottom velocity computation method)*

The governing equations for the main computational domain of the BVC method are derived from the continuity equation and the Reynolds-averaged Navier–Stokes equations assuming a vortex layer δz_b on the bed surface and a bottom velocity on the layer, as indicated in Figure 2. The depth-integrated continuity equation and horizontal momentum equations with vertical flux on the bottom are given as follows:

$$\frac{\partial h}{\partial t}+\frac{\partial U_j h}{\partial x_j}-w_{\sigma b}=0 \tag{1}$$

$$\frac{\partial U_i h}{\partial t}+\frac{\partial U_i U_j h}{\partial x_j}-w_{\sigma b}u_{bi}= -gh\frac{\partial z_s}{\partial x_i}-\frac{\tau_{bi}}{\rho}+\frac{\partial h T_{ij}}{\rho \partial x_j}-\left(\frac{\partial h\overline{dp}}{\rho \partial x_i}+\frac{dp_b}{\rho}\frac{\partial z_b}{\partial x_i}\right) \tag{2}$$

where i, j = 1(x),2(y); z: vertical direction; τ_{bi}: bottom shear stress; T_{ij}: horizontal shear stress; and $dp_0 = dp_b/2$. The horizontal shear stresses T_{ij}

Table 1. Unknown variables and equations.

	Unknown variables/equations	Equations
Main computational domain	h: water depth	DI continuity eq. (1)
	u_{si}: water surface velocity	Horizontal momentum eq. on water surface (9)
	U_i: depth averaged horizontal velocity	DI horizontal momentum eq. (2)
	W: depth averaged vertical velocity	Double integral of the continuity eq. of z (10)
	Ω_i: depth averaged horizontal vorticity	DI horizontal vorticity eq. (7)
	u_{bi}: bottom velocity	DI of definition eq. of horizontal vorticity (8)
	dp_b: bottom pressure deviation from the bottom hydrostatic pressure	DI vertical momentum eq. (11)
Vortex layer	$w_{\sigma b}$: bottom vertical flux	Continuity eq. for vortex layer (12)
	u_{vi}: horizontal velocity for vortex layer	Momentum eq. for vortex layer (13)
Roughness layer	$w_{\sigma t}$: bed surface vertical flux	Continuity eq. for roughness layer (12)
	u_{ri}: horizontal velocity for roughness layer	Momentum eq. for roughness layer (14)

DI: depth integrated

consist of shear stresses owing to molecular and turbulent motions and horizontal momentum transportation by vertical velocity distribution. $T_{ij} = \tau_{ij} + \overline{u_i' u_j'}$, $\tau_{ij} = \nu S_{ij}$, $\nu = \nu_m + \nu_t$, ν_m: kinematic viscosity coefficient, ν_t: the eddy viscosity coefficient, S_{ij}: depth-averaged strain velocity, and $u_i = U_i + u_i'$ (u_i: horizontal velocity). In this paper, an overline indicates a depth-integrated value. For the eddy viscosity coefficient, this study employs a one-equation model taking into account the velocity vertical distribution in the production term P_k (Uchida & Fukuoka, 2014):

$$\frac{\partial k}{\partial t} + U_j \frac{\partial k}{\partial x_j} = \frac{1}{h}\frac{\partial}{\partial x_i}\left(\frac{\nu h}{\sigma_k}\frac{\partial k}{\partial x_i}\right) + P_k - \varepsilon \tag{3}$$

where $\nu_t = C_\mu k^2/\varepsilon$, $C_\mu = 0.09$, $\varepsilon = C_\varepsilon k^{3/2}/\Delta$, $C_\varepsilon/\Delta = 1.7/h$ (Nadaoka & Yagi, 1998).

The cubic vertical velocity equation (4) is assumed by using the depth-averaged velocity U_i, the bottom velocity u_{bi}, and the water surface velocity u_{si} with the assumption of zero vertical velocity gradients at the water surface.

$$u_i' = \Delta u_i\left(12\eta^3 - 12\eta^2 + 1\right) + \delta u_i\left(-4\eta^3 + 3\eta^2\right) \tag{4}$$

where δu_i: $u_{si} - u_{bi}$, Δu_i: $u_{si} - U_i$, and $\eta = (z_s - z)/h$. The quadric curve of velocity distributions is used for the uniform flow, substituting $\Delta u_i = \delta u_i/3$ ($u_{sei} = U_i + \delta u_i/3$) in equation (4) (Uchida & Fukuoka, 2014).

To evaluate the vertical velocity and pressure distributions, the following equations are solved for the main calculation domain of the BVC method:

$$\frac{\partial \Omega_i h}{\partial t} = R_{\sigma i} + P_{\omega i} + \frac{\partial h D_{\omega ij}}{\partial x_j} + w_{\sigma b}\omega_{bi} \tag{7}$$

$$u_{bi} = u_{si} - \varepsilon_{ij3}\Omega_j h - \left(\frac{\partial Wh}{\partial x_i} - w_s\frac{\partial z_s}{\partial x_i} + w_b\frac{\partial z_b}{\partial x_i}\right) \tag{8}$$

$$\frac{\partial u_{si}}{\partial t} + u_{sj}\frac{\partial u_{si}}{\partial x_j} = -g^*\frac{\partial z_s}{\partial x_i} + P_{si} \tag{9}$$

$$Wh = h\left(\frac{\partial z_m}{\partial t} + U_i\frac{\partial z_m}{\partial x_i}\right) - \frac{\partial h^2\overline{\eta u_i'}}{\partial x_i} + hw_{\sigma b} \tag{10}$$

$$\frac{dp_b}{\rho} = \frac{\partial hWU_j}{\partial x_j} + \tau_{bj}\frac{\partial z_b}{\partial x_j} - \frac{\partial h\tau_{zj}}{\partial x_j} \tag{11}$$

where ε_{ijk}: Levi-Civita symbol, and w_s, w_b: vertical velocity on the water surface and bottom. The above equations with a time variation term calculate a time-advance scheme for each unknown variable in Table 1. The equations (8), (10), and (11), which do not include time variation terms, are calculated as follows. Before evaluating equation (11) for the bottom pressure difference dp_b, the velocity difference between the water surface, the bottom δu_i, and the vertical velocity integrated over the water depth Wh at the next time step are calculated to satisfy equations (8) and (10) at the $n + 1$ step, introducing a similar approach to the SMAC scheme for incompressible fluid. The details of the governing equations and numerical scheme for the main calculation domain of the BVC method may be found in Uchida & Fukuoka (2014).

2.3 *Dynamic rough wall law for the boundary conditions of the main computational domain*

Boundary conditions on the bottom for the main calculation domain should be given in the bed shear stress terms in momentum equations (2), and the production terms in vorticity equations (7)

with vertical flux $w_{\sigma b}$. The BVC method employing the equilibrium wall law (Uchida & Fukuoka, 2014) assumes the equilibrium velocity and vortex vertical distribution for the vortex layer, neglecting the vertical flux ($w_{\sigma b} = 0$). Those distributions for the vortex layer have been decided with the log law and bottom velocity. For the dynamic rough wall law, those boundary conditions are given dynamically with continuity and momentum equations for the vortex and roughness layers (Uchida et al., 2014), as shown in Figure 2.

$$w_{\sigma b} = w_{\sigma t} - \frac{\partial \delta z_b u_{vi}}{\partial x_i}, \quad w_{\sigma t} = -\frac{\partial \lambda \delta z_t u_{ri}}{\partial x_i} \tag{12}$$

$$\frac{\partial u_{vi}}{\partial t} + u_{vk}\frac{\partial u_{vi}}{\partial x_k} = -\frac{\partial (p_b + \rho g z_b)}{\rho \partial x_i} + \frac{\tau_{bi}}{\rho \delta z_b} - \frac{\tau_{ti}}{\rho \delta z_b} \tag{13}$$

$$\frac{\partial u_{ri}}{\partial t} + u_{rk}\frac{\partial u_{ri}}{\partial x_k} = -\frac{\partial (p_b + \rho g z_b)}{\rho \partial x_i} + \frac{\tau_{ti}}{\rho \delta z_r} - \frac{D_i}{\rho \delta z_r} \tag{14}$$

where λ: porosity in the roughness layer ($\lambda = 0.4$); $k = 1,2,3$; p_b: bottom pressure $p_b = \rho g h + dp_b$; τ_{bi}, τ_{ti}: shear stress acting on the bottom and roughness layer surface; δz_b, δz_r: the thickness of the vortex and roughness layers; D_i: resistance term owing to drag force acting on roughness. The shear stress acting on the lower surface of the roughness layer is neglected in equation (14). The roughness layer thickness is assumed as $\delta z_r = k_s$ in this paper.

The shear stress and resistance terms in the momentum equations for the vortex and roughness layers are derived so that the DWL reduces to the EWL for the equilibrium condition. The shear stress acting on the vortex layer can be assumed based on the Boussinesq approximation:

$$\frac{\tau_{bi}}{\rho} = \left(\nu_t \frac{\partial u_i}{\partial z}\right)_b = \nu_{tb} \cdot A_b \frac{(u_{bi} - u_{vi})}{h} \tag{15}$$

The coefficients A_b are decided to satisfy $\tau_b = \rho u_*^2$ ($\tau_b^2 = \tau_{bi}\tau_{bi}$), $u_* = u_b/c_b = u_v/c_v$, and $\nu_{tb} = \alpha u_* h$ for the equilibrium condition by introducing the conventional logarithmic velocity law:

$$1/A_b = \alpha(c_b - c_v) = (\alpha/\kappa)\ln(z_b/z_v) \tag{16}$$

where $z_b = \delta z_0 + \delta z_b$, $z_v = \delta z_0 + \delta z_b/2$, δz_0: depth of the log law origin from the top of the roughness height, $\delta z_0 = 0.3 k_s$. The eddy viscosities for evaluating shear stress acting on the bottom are expressed by using the distance of the wall and velocity difference:

$$\nu_{tb} = \alpha_b \delta u_b h, \quad \delta u_b^{\,2} = (u_{bi} - u_{vi})(u_{bi} - u_{vi}) \tag{17}$$

where the coefficient α_b is given by $\alpha_b = \alpha/(c_b - c_v) = A_b$ to reduce $\nu_{tb} = \alpha u_* h$ for the equilibrium condition. However, using bottom vorticity ω_b gives another expression of the bottom eddy viscosity ν_{tb}:

$$\nu_{tb} = \frac{\alpha \kappa \omega_b h^2}{2\ln(z_s/z_b)} \tag{18}$$

This study uses the larger value between equations (17) and (18).

In a similar manner, the shear stress and the eddy viscosity on the bed surface (the top of the roughness layer) are given as

$$\frac{\tau_{ti}}{\rho} = \nu_{tt} \cdot A_t \frac{(u_{vi} - u_{ri})}{h}\left(\frac{h + \delta z_b}{h}\right) \tag{19}$$

$$\nu_{tt} = \alpha_t \delta u_t h, \quad \delta u_t^{\,2} = (u_{vi} - u_{ri})(u_{vi} - u_{ri}) \tag{20}$$

$$1/A_t = 1/\alpha_t = \alpha(c_v - c_r) \tag{21}$$

where $c_v = (1/\kappa)\ln(z_v/k_s) + A_r$, $A_r = 8.5$, $u_* = u_t/c_r$. For the equilibrium condition, since the right-hand side of equation (14) is zero, the magnitude of the resistance term should be represented by $D = \tau_t + \rho g \delta z_r S$ (S: channel slope). The coefficient c_r is evaluated with the resistance term of equation (14), when we introduce a drag coefficient to represent the resistance term:

$$c_r = \sqrt{\frac{8}{\pi C_D}\left(1 + \frac{\delta z_r + \delta z_b}{h}\right)} \tag{22}$$

$$D_i = \frac{\pi C_D}{8} \rho u_r u_{ri} \tag{23}$$

where $C_D = 0.4$.

The production terms $P_{\omega i}$ in equation (7) are given by equation (24) (Uchida & Fukuoka, 2014).

$$P_{\omega i} = C_{p\omega} \nu_{tb} (\omega_{bei} - \omega_{bi})/h + P_{s\omega i} \tag{24}$$

where $C_{p\omega} = \kappa/\alpha$, ω_{bi}: horizontal vorticity on bottom, ω_{bei}: equilibrium ω_{bi}, $P_{s\omega i}$: vorticity production owing to flow separation (Uchida & Fukuoka, 2011, 2014). The equilibrium vorticity on the production term in the vorticity equation (11) is assumed by using a velocity gradient in vorticity in the layer as

$$\omega_{bej} = \varepsilon_{ij3} A_\omega \frac{u_{bi} - u_{vi}}{h} \tag{25}$$

where the coefficient A_ω is represented by equation (26) so that equation (25) reduces to equation (27) for the equilibrium condition.

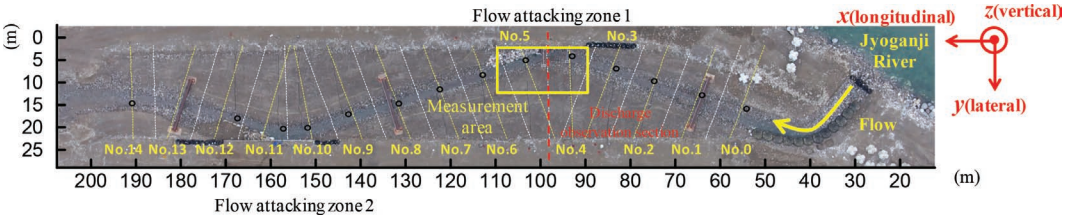

Figure 3. Plan view of the experimental channel (Koshiishi et al., 2012, 2013).

$$A_\omega = \frac{2}{\kappa(c_b - c_r)} \ln\left(\frac{z_s}{z_b}\right) \tag{26}$$

$$\omega_{be} = \frac{2u_*}{\kappa h} \ln\left(\frac{z_s}{z_b}\right) \tag{27}$$

3 FIELD MEASUMENT AND 3D LOCAL FLOW MEASUREMENT USING ADCP

A field experiment in the Jyoganji River in 2011 was conducted to investigate characteristics of erosion and bed scouring beside a revetment works (Koikeda *et al.*, 2012), and to obtain detailed data to validate the new depth-integrated calculation method for bed scouring in a flow attacking area (Koshiishi et al., 2012, 2013). The experiments were conducted in a compound meandering channel with total channel length: 170.0 m, total channel width: 20.0 m, main channel width: 4.0 m, main channel depth: 1.0 m, and bed slope: 1/200. The experimental discharge was 7.6 m^3/s. There are vertical revetments made with concrete walls in two flow attacking zones around meandering sections (Figure 3). The three-dimensional components of velocities by means of ADCP were measured around the flow attacking zone 1.

The conventional method of ADCP calculates a velocity vertical profile with four different direction beams (Teledyne RD Instruments, 2006). It cannot give accurate local velocity vectors for flows with large velocity gradients and deep water depth. This is because of velocity variations within the focus spot L surrounded by four beams, which expands toward the vertical direction by an angle of 20°, as shown in Figure 4.

To obtain accurate local 3D velocity distribution around a structure, individual beam data in each direction for current profiles of the ADCP are managed as follows (Koshiishi et al., 2012, 2013). Koshiishi et al. (2012, 2013) calculated the lateral and vertical velocity at any point using superimposing spatially interpolated individual beam data, which are measured continuously in the lateral direction and are averaged over time as shown in Figure 5. Variations in the stream-wise

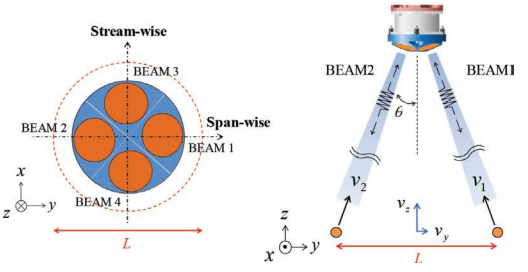

Figure 4. Concept of the conventional ADCP method (Koshiishi et al., 2012, 2013).

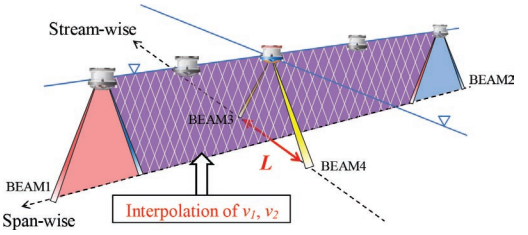

Figure 5. Concept of the present ADCP method (Koshiishi et al., 2012, 2013).

velocity component are assumed to be negligibly small compared with those of the lateral and vertical directions. Koshiishi et al. (2012) have shown that this method could measure 3D local flows in front of a revetment with accuracy, especially in the vicinity of the bed surface. The details of the measuring method and experiments may be found in Koshiishi et al. (2012, 2013).

4 COMPUTED RESULTS AND DISCUSSIONS

We applied the BVC-DWL to the real scale 3D flow in front of a structure measured in the Joganji River field experiment. Figure 6 shows a comparison of the water surface and bottom velocity between measured (Koshiishi et al., 2012, 2013) and calculated (BVC-DWL) results. We can see in

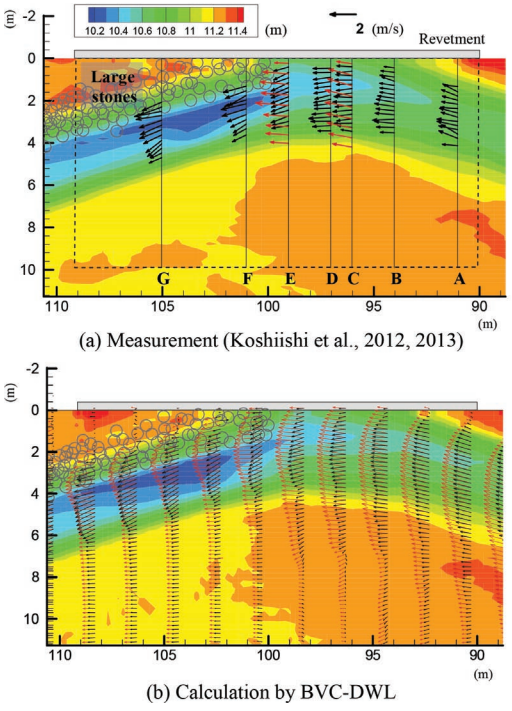

Figure 6. Comparisons of water surface and bottom velocity between measured (Koshiishi et al., 2012, 2013) and calculated (BVC-DWL) results.

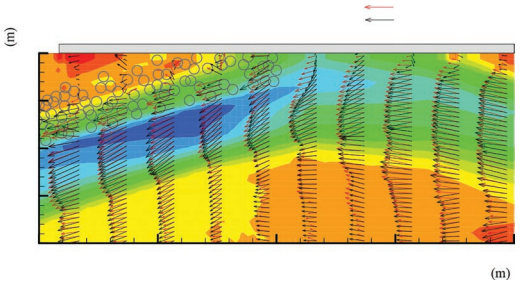

Figure 7. Comparisons of calculated velocity distributions in the roughness layer between BVC-EWL and BVC-DWL.

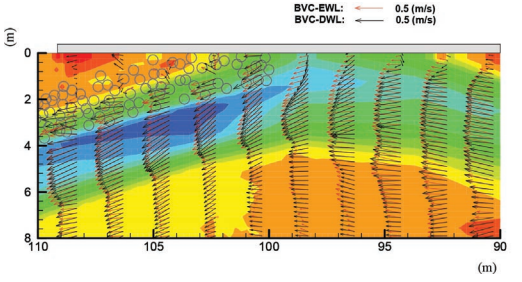

Figure 8. Comparisons of local 3D velocity distributions on flow attacking zone between measured (Koshiishi et al., 2012, 2013) and calculated (BVC-EWL, BVC-DWL) results.

the measured results that the bottom velocity vectors were bent toward the inner bank, while the water surface velocity vectors move in the direction of the outer bank. These characteristics measured in the field experiment are well explained by the calculation results of the BVC-DWL method.

Figure 7 shows comparisons of calculated velocity distributions in the roughness layer between BVC-EWL and BVC-DWL. The large difference that occurs by introducing DWL can be seen around outer bank, in which the roughness layer velocity of BVC-DWL is bent toward the inner bank owing to the strong downward flux of the secondary flow, while the velocity of BVC-EWL does not have as much of an inner bank component.

The above numerical investigation indicates the flow pattern under the bottom varies considerably for the local 3D flow around a structure in gravel bed rivers. Figure 8 shows comparisons of local 3D velocity distributions on a flow attacking zone between measured (Koshiishi et al., 2012, 2013) and computed (BVC-EWL, BVC-DWL) results. In the calculated results, bed heights are set to z_t, and the velocity distribution between z_s and z_t is shown. The velocity vectors on the bottom z_b are third vectors from the bed.

The measured results indicate the 3D flow characteristics as follows. We can find weak secondary flows near the bottom on the right bank for the approaching flow (Section B). For the flow attacking zone of Sections C–E, clockwise secondary flows are developed in the entire cross section. For Sections F and G, large stones bend flows near the bed toward the inner bank. The above 3D flow characteristics in the experiment are explained by the calculated results using BVC-EWL. However, the calculated secondary flows are underestimated by BVC-EWL. The main velocity areas do not shift to the outer bank for Sections C–F compared with those of the experiment. The calculated results of BVC-DWL demonstrate that the above problems of BVC-EWL are considerably improved by introducing DWL, even though some differences between BVC-DWL and measurements can be found.

5 CONCLUSIONS

This paper presents a non-hydrostatic depth-integrated model, the general Bottom Velocity Computation method, which employs the dynamic rough wall law (BVC-DWL). The local 3D flows

around a structure in a gravel bed river measured with the enhanced measurement method using the Acoustic Doppler Current Profiler (ADCP) are compared with the BVC-DWL method. The water surface and bottom velocity distributions calculated by BVC-DWL are in good agreement with those of the measurement. The roughness layer velocity distribution with BVC-DWL differs from the calculation result that employs the conventional equilibrium rough wall law (BVC-EWL) around a structure owing to the downward flux of the secondary flow. This paper presents local 3D velocity distributions in several cross sections around the structure in the gravel bed river measured by enhanced ADCP. The detailed comparisons with measured results indicate the problems of BVC-EWL in which secondary flows are underestimated and the main velocity areas do not shift to the outer bank. Although there are some differences between BVC-DWL and the measurements, the BVC-DWL is able to improve the above problems of BVC-EWL considerably.

REFERENCES

Fukuoka, S., Watanabe, A., and Nishimura, T. (1992) "On the groin arrangement in meandering rivers" Journal of Hydraulic Engineering, JSCE, No. 443/II-18, pp. 27–36, in Japanese.

Fukuoka, S. and Uchida, T. (2013) "Toward integrated multi-scale simulations of flow and sediment transport in rivers" Journal of JSCE Ser. B1 (Hydraulic Engineering) 69(4): II-1–II-10.

Koikeda, S., Ishii, A., Iwai, H., Ishikawa, T., and Fukuoka, S. (2012) "Nature friendly bank protection works using sandbars with boulders in the Jyoganji river," Advances in River Engineering 18: 233–238, JSCE, in Japanese.

Koshiishi, M., Uchida, T. and Fukuoka, S. (2012) "A New method for measuring local Flows around river bank using ADCP" Proceedings of the 10th International Conference on Hydroscience & Engineering, Orlando, FL, USA.

Koshiishi, M., Uchida, T. and Fukuoka, S. (2013) "A new method for measuring and calculating flows and bed forms around river banks" Advances in River Sediment Research, Proceedings of 12th International Symposium on River Sedimentation, ISRS-2016, Kyoto, Japan.

Ishikawa, T., Suzuki, K. and Tanaka, M. (1986) "Efficient numerical analysis of an open channel flow with secondary circulations" Proc. of JSCE 375/II-6: 181–189.

Jin Y.-C. and Steffler, P.M. (1993) "Predicting flow in curved open channels by depth-averaged method" J. Hydraul. Eng. 119(1): 109–124.

Lane, S.N., Hardy, R.J., Elliott, L., and Ingham, D. B. (2004) "Numerical modeling of flow processes over gravelly surfaces using structured grids and a numerical porosity treatment," Water Recourses Research 40: W01302.

Nadaoka, K. and Yagi, H. (1998) "Shallow-water turbulence modeling and horizontal large-eddy computation of river flow" Journal of Hydraulic Engineering 124(5): 493–500.

Nikora, V., McEwan, I., McLean, S., Coleman, S., Pokrajac, D., and Walters, R. (2007a) "Double-averaging concept for rough-bed open-channel and overland flows: Theoretical background," J. Hydraul. Eng 133: 873–883.

Nikora, V., McLean, S., Coleman, S., Pokrajac, D., McEwan, I., Campbell, L., Aberle, J., Clunie, D., and Koll, K. (2007b) "Double-averaging concept for rough-bed open-channel and overland flows: Applications," J. Hydraul. Eng 133: 884–895.

Olsen, N.R.B. and Stokseth, S. (1995) "Three-dimensional nu-merical modelling of water flow in a river with large bed roughness" Journal of Hydraulic Research 33(4): 571–581.

Teledyne RD Instruments (2006) "Acoustic Doppler current profiler principles of operation a practical primer."

Uchida, T. and Fukuoka, S. (2011) "A bottom velocity computation method for estimating bed variation in a channel with submerged groins" Journal of JSCE, Ser. B1 (Hydraulic Engineering), 67(1): 16–29, in Japanese.

Uchida, T. and Fukuoka, S. (2012) "Bottom velocity computation method by depth-integrated model without shallow water assumption" Journal of JSCE, Ser. B1 (Hydraulic Engineering) 68(4): I_1225–I_1230, in Japanese.

Uchida, T. and Fukuoka, S. (2014) "Numerical calculation for bed variation in compound-meandering channel using depth in-tegrated model without assumption of shallow water flow" Advances in Water Resources 72: 45–56.

Uchida, T., Fukuoka, S., Papanicolaou, A.N., and Tsakiris, A.G.(2014) "A numerical calculation method for flow in the presence of isolated boulders atop a rough bed by using an enhanced depth-integrated model with a non-equilibrium resistance law" Proceedings of International Conference on Fluvial Hydraulics, River Flow, Lausanne, Switzerland, pp. 335–343, 2014.

Yeh, K.-C. and Kennedy, J.F. (1993) "Moment model of nonuniform channel-bend flow. I: Fixed beds" J. Hydraul. Eng. 119(7): 776–795.